International Journal of Statistics and Applied Mathematics 2026; 11(1): 100-115

International Journal of Statistics and Applied Mathematics

ISSN: 2456-1452
NAAS Rating (2025): 4.49
Maths 2026; 11(1): 100-115
© 2026 Stats & Maths
https://www.mathsjournal.com
Received: 05-10-2025
Accepted: 14-11-2025

Hemawati
Government First Grade College, Bhalki, Karnataka, India

Mahesh Kudrikar
Smt. Kamal Basawaraj Patil Okaly Degree College, Kalaburagi, Karnataka, India

Corresponding Author:
Hemawati
Government First Grade College, Bhalki, Karnataka, India

Numerical analysis of electro conductive Nano-fluid flow and thermal transport over a moving surface with heat generation and absorption

Hemawati and Mahesh Kudrikar

DOI: https://www.DOI.org/10.22271/maths.2026.v11.i1b.2244

Abstract
In this paper, a theoretical exercise on conducting nanofluid flow on a stretching sheet in the presence of a heat source/sink is investigated. A Buongiorno nanoscale formulation is developed to define the nanofluid model. By using an appropriate similarity transformation, the nonlinear partial differential equations are transformed into a nonlinear ordinary differential equation. The transformed system of differential equations is numerically solved using a MATLAB program. The effects of the blade velocity parameter, magnetic field parameter, Brownian motion parameter, thermophoresis parameter, Prandtl number, magnetic Prandtl number, thermal radiation parameter, Lewis number and heat source/sink parameter on the velocity, induced magnetic stream function gradient, temperature and nanoparticle concentration have been studied and presented graphically. The physical parameters such as skin friction function, local Nusselt number and Sherwood numbers are also computed and presented in tabular form. It is found that blade velocity parameter and magnetic Prandtl number increases the velocity whereas the magnetic field parameter suppresses the velocity. The temperature is enhanced with the Brownian motion, thermophoresis, parameter, radiation and heat source parameters and is suppressed with Prandtle number and heat sink parameters.

Keywords: Nanofluid, MHD, convection, induction, stretching sheet, buongiorno model, source/sink

1. Introduction

In recent years, research on nanofluidic flows has attracted great interest of researchers due to increased implementations in various fields of technology, science, bio-mechanics, chemistry and nuclear industry. The term nanofluid means adding a smaller amount of nanometer-sized particles nominally below 100 nm to base fluids such as oil, water, bio fluids and ethylene and lubricant. The term was first introduced by Choi *et al.* [1]; he added tiny nanoparticles to the base fluid to increase the thermal conductivity. Uddin *et al.* [2] Research on radiative Convective Nano fluid Flow past a Stretching/ Shrinking Sheet with Slip Effects. The purpose of this study is to improve the thermo physical properties of convection and heat transfer of unsteady nanoliquids through moving Stretching/Shrinking Sheet in the presence of Radiative Convective Nanofluid. B. Mahanthesh *et al.* [3] analytically investigated the effect of an induced magnetic field on a flat porous plate using an incompressible copper-water nanofluid. The flow should be laminar, stable, and two-dimensional. The plate is subject to normal free flow and suction velocities. Aamir Ali *et al.* [4] investigated on electro-magneto hydrodynamic nanofluid flow with radiation and variable heat flux impact on a slender tension sheet. It has been observed that linear stretching sheets have been extensively used in heat transfer research.

In recent years, MHD fluid flow has attracted the attention of researchers due to controllable heat transfer coefficient. Magnetohydrodynamics plays a decisive role in controlling the cooling rate and melt separation. The term "magnetohydrodynamics" is a combination of his three basic terms: magneto for magnetic fields, hydro for fluids/liquids and dynamics for particle evolution. Vikas Poply [5] analyzed the heat transfer characteristics in a Magnetohydrodynamic (MHD) boundary layer nanofluid flow over a stretching sheet.

They found that the skin friction coefficient increases with increasing magnetic parameter M. Ahmad *et al.* [6] numerically investigated the effects of thermal radiation and heat generation on the flow of conducting magnetic nanofluid through nonlinear stretchable films through porous media via frictional heating. Study of flow and heat transfer in permeability stretch magnetohydrodynamic nanofluidic sheets under the influence of convection boundary conditions is discussed by B. Srisailam *et al.* [7]. They observed that the thickness of the boundary layer reduces as the magnetic parameter (M) increases, whereas the temperature and concentration profile increase. Sonika Sharma *et al.* [8] investigated an exponentially stretched sheet with a magnetic force to explore the Darcy-Forchheimer flow of a two-dimensional blood-based nanofluid and the effect of different relevant parameters of the fluid flow assumption for velocity and temperature profiles.

The mixed convection laminar flow of couple stress fluid induced by oscillatory stretching sheet in presence of nanoparticles has been investigated analytically by Shankar *et al.* [9]. Daniel *et al.* [10] studied the combined effects of thermal stratification, applied magnetic field, and thermal radiation on a boundary layer flow of electrically conducting nanofluid over a nonlinear stretching sheet. The radiative heat transfer is to be sensitive to an increase in the fluid temperature and thicker thermal boundary layer thickness. Thin layer mechanisms are often used to improve the surface properties of solids. Penetration, degradation, stiffness, illumination, diffusion, absorption, and electrical performance are all properties of bulk media that can be enhanced by thin films. So for this the time-dependent nonlinearly convective flow in thin film nanoliquid over an inclined stretchable sheet with magnetic effects was investigated by Anwar *et al.* [11]. Iskandar *et al.* [12] considered the mixed convection and heat transfer across exponentially stretching vertical planes in hybrid nanofluids. They observed that the heat transfer rate enhances in the presence of nanoparticles.

The effect of the induced magnetic field on the motion of nanofluid Al2O3 containing rotationally moving microbes through the boundary layer is examined by Nabil *et al.* [13].They found that increases in velocity profiles shows increase in M and the Grashof number. While it decreases with an increase in the reciprocal magnetic Prandtl number. Oyier *et al.* [14] investigated the effect of induced magneticfield on the MHD laminar flow of oldroyd-B nanofluid over elongating surface and heat producing. It was found that the external magnetic field perpendicular to layer affects the fluid flow. Flow and heat transfer induced by exponentially shrinking hybrid films Nano particles are studied by Iskandar *et al.* [15]. Aluminum oxide (Al2O3) and copper (Cu) nanoparticles are suspended in water to form an Al2O3-Cu/water hybrid nanofluid. Anwar *et al.* [16] analysied the study on the induced magnetic field applied by the exponentially stretched plates to the flow of second-class fluids with different thermal conductivities. They considered chemical reactions and viscous dissipation effects under the influence of thermophoresis and Brownian motion on exponentially stretched sheets.

Alblawi *et al.* [17] studied on steady flow of Buongiorno's model on the exponentially stretching surface. The aim of the study was to analyze the heat transfer coefficient of nanoliquids on momentum boundary layer thickness, thermal boundary layer thickness, and solution boundary layer thickness are astonishing. Flow and heat transfer through Shrinking Sheet using a modified Buongiorno nanoliquid model by Natalia *et al.* [18]. They used both nanofluidic flow and hybrid nanofluidic flow (the so-called modified Bongiorno nonliquid model) to study the heat transfer properties across boundary layer flows and permeable isothermal stretch surfaces. Aldabesh *et al.* [19] studied thermally variable conductivity features in a Buongiorno nanofluid model between parallel stretching discs (energy improvement system efficiency).

The study of heat generation or absorption in moving liquids is important for problems related to liquid dissociation. Temperature distribution may change due to heat generation. This determines the deposition rate of particles in nuclear reactors, electronic chips and semiconductor wafers. Kerur *et al.* [20] investigated on the effects of thermal radiation and chemical reactions heat and mass transfer in Mhd cassion nanofluid flow passes through a stretching sheet under the influence of heat source/sink. For positive values of the parameter n the heat source/sink acts as a heat generator and for negative values of the parameter the heat source/sink acts as a heat sink from the boundary layer. Thiagarajan *et al.* [21]. Analyzed on nanofluid hydromagnetic boundary layer flow and heat transfer across porous exponentially stretching sheets with effects on heat generation/absorption and ohmic heating. Increasing the magnetic interaction parameter, heat source parameter, Eckert number, thermal radiation parameter, and Brownian motion increases the dimensionless temperature in the boundary layer region, but decreases the heat sink parameter in temperature. Effects of magnetic fields on heat generation and absorption flow of nanofluids across nonlinear stretch films by Santoshi *et al.* [22]. They observed that heat generation coefficient is responsible for changing the heat gradient of the fluid flow, which has a negligible influence on the concentration levels of the fluid particle.

The above studies do not take into account the magnetic induction effect that occurs at higher magnetic Reynolds numbers. MHD nanomaterial processing. Furthermore, thermal radiation is important in high temperature nanomaterials processing. The effect of embedding parameters, ie. Blade velocity parameter λ, magnetic field parameter β, Prandtl number Pr, magnetic Prandtl number Prm, thermal radiation parameter Rd, Lewis number Le, Brownian motion parameter Nb and thermophoretic parameter Nt, heat absorption (sink) parameter for velocity (Φ), induced magnetic field, temperature, nanoparticle concentration, skin friction, local Nusselt number and Sherwood number profiles are visualized. Includes residual error analysis for convergence rate and repetition rate. Therefore, the novelty of this work is that we have considered a large number of different nanoparticles for magnetic nanofluids, including thermal radiation, nanoparticle concentration, and heat source/sink effects.

2. Mathematical formulation of the problem

Figure 1 delineate the regime under the study of Two-Dimensional, viscous MHD thermal convection boundary layer flow of an electrically conducting nanofluid from a moving semi-infinite surface (sheet).

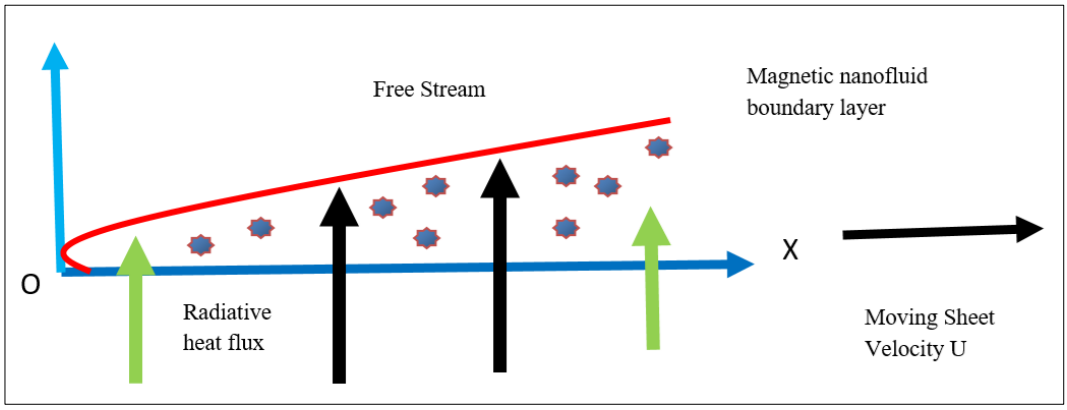

Fig 1: Magnetic induction nanofluid radiative convection physical model

The physical model is shown in Figure 1. A uniform magnetic field of force H_0 is applied to the surface in the normal direction. The component of the induced magnetic field H_2 disappears when it hits the wall and the parallel component H_1 approaches the value of H_0. An (x, y) coordinate system is adopted. It is also assumed that the velocity of the free stream is U, and that of the plate (sheet) is $U_w = \lambda U$, where λ is a velocity parameter. At the moving surface, the temperature and the nanoparticle concentration take constant values T_w and C_w, respectively, while the free stream values are prescribed as T_∞ and C_∞, respectively. Under the boundary layer approximations, using the Buongiorno two-component nanoscale model [23] and Heat sink/source [21], the conservation equations can be written as follows.

$$\frac{\partial u}{\partial x} + \frac{\partial v}{\partial y} = 0 \tag{1}$$

$$\frac{\partial H_1}{\partial x} + \frac{\partial H_2}{\partial y} = 0 \tag{2}$$

$$u\frac{\partial u}{\partial x} + v\frac{\partial u}{\partial y} = \nu\frac{\partial^2 u}{\partial y^2} + \frac{\mu_0}{\rho}\left(H_1\frac{\partial H_1}{\partial x} + H_2\frac{\partial H_2}{\partial y}\right) \tag{3}$$

$$u\frac{\partial H_1}{\partial x} + v\frac{\partial H_1}{\partial y} - H_1\frac{\partial u}{\partial x} - H_2\frac{\partial u}{\partial y} = \alpha_1\frac{\partial^2 H_1}{\partial y^2} \tag{4}$$

$$u\frac{\partial T}{\partial x} + v\frac{\partial T}{\partial y} = \alpha\frac{\partial^2 T}{\partial y^2} - \frac{\alpha}{K}\frac{\partial q_r}{\partial y} + \tau\left(D_B\frac{\partial C}{\partial y}\frac{\partial T}{\partial y} + \left(\frac{D_B}{T_\infty}\right)\left(\frac{\partial T}{\partial y}\right)^2\right) + Q\frac{(T - T_w)}{(\rho cp)_f} \tag{5}$$

$$u\frac{\partial C}{\partial x} + v\frac{\partial C}{\partial y} = D_B\frac{\partial^2 C}{\partial y^2} + \left(\frac{D_B}{T_\infty}\right)\left(\frac{\partial^2 T}{\partial y^2}\right) \tag{6}$$

where u and v are the velocity components along the x-axis and the y-axis, respectively, T is the nanofluid temperature, ρ and ν are the nanofluid density, μ_0 is the magnetic permeability, α_1 is the magnetic diffusivity, $\alpha = K/(\rho cp)_f$ is the thermal diffusivity of the fluid, K is the thermal conductivity of magnetic nanofluid, $(\rho cp)_f$ is the heat capacity of the base fluid, q_r is the heat flux, ρ is the Brownian diffusion coefficient, D_T is the thermophoresis diffusion coefficient, $\tau = (\rho cp)_p / (\rho cp)_f$, and $(\rho cp)_p$ is the heat capacity of the nanoparticles. The radiative heat flux q_r is evaluated by using Rosseland diffusion approximation.

$$q_r = \frac{4\sigma^*}{3K_s}\frac{\partial T^4}{\partial y} \tag{7}$$

Where σ^* and K_s are the Stephan-Boltzman constant and the Rosseland mean absorption coefficient, respectively. The temperature differences within the flow are sufficiently small under the assumption that T_s may be expressed as a linear combination of the temperature as shown in Chamakha *et al.* [27]. Expanding T_4 in a Taylor series about T_∞ and neglecting the higher order terms, we obtain

$$T^4 \cong 4T_\infty^3 T - 3T_\infty^4 \tag{8}$$

Using

$$\frac{\partial q_r}{\partial y} = \frac{16\sigma^* T_\infty^3}{3K_s}\frac{\partial^2 T}{\partial y^2} \tag{9}$$

The prescribed boundary conditions at the wall (plate) and in the free stream for equations (1)-(6) are defined as follows:

At Y=0

$$u = \lambda U,\ v = 0,\ \frac{\partial H_1}{\partial y} = H_2 = 0,\ T = T_w,\ C = C_w \tag{10.a}$$

At $Y \to \infty$

$$u \to U,\ H_1 \to H_0,\ T \to T_\infty,\ C \to C_\infty \tag{10.b}$$

3. Similarity Transformations

We now introduce the following similarity transformations, to normalize the boundary layer equations:

$$\psi = (2Uvx)^{\frac{1}{2}} f(\eta),\ \phi = \left(\frac{2vx}{U}\right)^{\frac{1}{2}} H_0 g(\eta),\ \eta = \left(\frac{U}{2vx}\right)^{\frac{1}{2}} y$$

$$\theta(\eta) = \frac{(T - T_w)}{(T_w - T_\infty)},\ \varphi(\eta) = \frac{(C - C_w)}{(C_w - C_\infty)} \tag{11}$$

Here, ψ is the stream function, which is defined as $u = \partial\psi/\partial y$ and $v = -\partial\psi/\partial x$, and ϕ is the magnetic stream function, defined by $H_1 = \partial\phi/\partial y$ and $H_2 = -\partial\phi/\partial x$, Further, η is the dimensionless similarity variable, f and g are dimensionless stream and magnetic stream functions, respectively, θ is the dimensionless temperature function, and ϕ is the dimensionless Nano particle concentration. Mass conservation and magnetic field continuity are satisfied identically. Substituting the similarity variables into equations (3) - (6) gives the following similarity ordinary nonlinear differential momentum, magnetic, thermal, and species nanoparticles (nanoparticle) boundary layer equations:

$$f''' + ff'' - \beta g g'' = 0 \tag{12}$$

$$\frac{1}{\Pr m} g''' + fg'' - gf'' = 0 \tag{13}$$

$$\left(\frac{3 + 4Rd}{3\Pr}\right)\theta'' + f\theta' + Nb\theta'^{\psi'} + Nt(\theta')^2 + \Phi\theta = 0 \tag{14}$$

$$\psi'' + Lef\psi' + \left(\frac{Nt}{Nb}\right)\theta'' = 0 \tag{15}$$

The dimensionless boundary conditions for the tenth-order problem now become

$$f(0)=0,\ f'(0)=\lambda,\ g(0)=0=g''(0)=0,\ \theta(0)=1,\ \psi(0)=1\ \eta=0 \tag{16.a}$$

$$f'\to 1,\ g'\to 1,\ \theta'\to 0,\ \psi'\to 0\ \ \eta\to\infty \tag{16.b}$$

Here, primes denote differentiation with respect to η, f' is the dimensionless velocity, g' is the dimensionless induced magnetic field stream function gradient, $\Pr=\nu/\alpha$ is the Prandtl number, $\Pr m=\nu/\alpha_1$ is the magnetic Prandtl number, $\beta=\mu_0 H_0^{\ 2}/\rho U^2$ is the magnetic body force number, $Rd=4\sigma^* T_\infty^{\ 3}/KK_s$ is the radiation parameter, $Nb=(\tau D_B/\nu)(C_w-C_\infty)$ is the Brownian motion parameter, $Nt=(\tau D_T/\nu T_\infty)(T_w-T_\infty)$ is the thermophoresis parameter, and $Le=\nu/D_B$ is the Lewis number. The physical quantities of interest in magnetic material processing are the skin-friction coefficient C_f, the local Nusselt number Nu_x, and the local Sherwood number Sh_x. These parameters, respectively, characterize the surface drag, wall heat transfer rate, and wall nanoparticle mass transfer rate.

The skin-friction coefficient is defined as

$$C_f=\frac{\tau_w}{\rho U^2} \tag{17}$$

Here, τ_w is the shear stress at the surface of the wall (sheet), which is given by

$$\tau_w=u\left[\frac{\partial u}{\partial y}\right]_{y=0}=\rho U^{\frac{3}{2}}\sqrt{\frac{\nu}{2x}}f''(0) \tag{18}$$

Using equation (18) in (17), we obtain the dimensionless skin friction coefficient (surface drag) as.

$$\sqrt{2\,\mathrm{Re}_x}C_f=f''(0) \tag{19}$$

The Nusselt number is defined as

$$Nu_x=\frac{xq_w}{K(T_w-T_\infty)} \tag{20}$$

Where the heat transfer rate at the surface is given by

$$q_w=-K\left[\frac{\partial T}{\partial y}\right]_{y=0}=-K(T_w-T_\infty)\sqrt{\frac{U}{2\nu x}}\theta'(0) \tag{21}$$

Using equation (21) in (20), the dimensionless wall heat transfer rate is obtained as

$$\sqrt{\frac{2}{\mathrm{Re}_x}}Nu_x=-\theta'(0) \tag{22}$$

The nanoparticle mass transfer rate at the surface is given by

$$q_m=-D_B\left[\frac{\partial C}{\partial y}\right]_{y=0}=-D_B(C_w-C_\infty)\sqrt{\frac{U}{2\nu x}}\varphi'(0) \tag{23}$$

The Sherwood number is defined as

$$Sh_x=\frac{xq_m}{D_B(C_w-C_\infty)} \tag{24}$$

From equations (23) and (24), the dimensionless nanoparticle mass transfer rate becomes

$$\sqrt{\frac{2}{\mathrm{Re}_x}}Sh_x = -\varphi^{'}(0) \tag{25}$$

4. Numerical Methods

A nonlinear ordinary derivative boundary value problem defined by equations (12)-(15) can be solved using a number of numerical methods, including finite elements, finite differences, etc. Here, we choose the MATLAB BVP4C routine (boundary value problem), which uses aexceptionally accurate method. This technique has been applied to many multiphysics fluid dynamics problems by Umavathi *et al.* [23]. In this study, the following fixed parameter values are adopted for computations: Pr = 0.7, Prm = 0.5, λ= 0.1, β= 0.1, Nt = 0.1, Nb = 0.3, Rd = 0.5, and Le = 5. In MATLAB this quadrature is used to obtain solutions for velocity profile, Incuced magnetic stream function, and temperature and Nanoparticle concentration. BVP4C uses stepping formulae which are summarized in Nayema *et al.* [24], comparison has been made with Shateyi and Prakash *et al.* [25] and Shahina Akter *et al.* [26].

Simulations of the transformed Eqns (12-15) subject to the boundary conditions (16a) - (16b) are found with the help of MATLAB BVP4C numerical method for various values of the flow controlling parameters. In the context of bvp4c function described above we need to transform the governing equations into first order differential equation. At first Eqns (12-15) can be rearranged in the following way.

$$f^{'''} = \beta g g^{''} - f f^{''}$$

$$g^{'''} = \mathrm{Pr}\, m(g f^{''} - f g^{''})$$

$$\theta^{''} = -\left(\frac{3\mathrm{Pr}}{3+4Rd}\right)(f\theta^{'} + Nb\theta^{'}\psi^{'} + Nt(\theta^{'})^2 + \Phi\theta)$$

$$\psi^{''} = -Lef\psi^{'} - \left(\frac{Nt}{Nb}\right)\left(-\left(\frac{3\mathrm{Pr}}{3+4Rd}\right)(f\theta^{'} + Nb\theta^{'}\psi^{'} + Nt(\theta^{'})^2 + \Phi\theta)\right)$$

Now we need to transform this above equation into first order differential equation.

$$f = y_1,\ f^{'} = y_2,\ f^{''} = y_3,\ g = y_4,\ g^{'} = y_5,\ g^{''} = y_6$$

$$\theta = y_7,\ \theta^{'} = y_8,\ \varphi = y_9,\ \varphi^{'} = y_{10}$$

The corresponding first order differential equations are

$$\frac{dy_1}{dx} = y_2$$

$$\frac{dy_2}{dx} = y_3$$

$$\frac{dy_3}{dx} = \beta y_4 y_6 - y_1 y_3$$

$$\frac{dy_5}{dx} = y_6$$

$$\frac{dy_6}{dx} = \mathrm{Pr}\, m(y_4 y_3 - y_1 y_6)$$

$$\frac{dy_7}{dx} = y_8$$

$$\frac{dy_8}{dx} = -\left(\frac{3\Pr}{3+4Rd}\right)(y_1 y_8 + Nby_8 y_{10} + Nt(y_8)^2 + \Phi y_7)$$

$$\frac{dy_9}{dx} = y_{10}$$

$$\frac{dy_{10}}{dx} = -Ley_1 y_{10} - \left(\frac{Nt}{Nb}\right)\left(-\left(\frac{3\Pr}{3+4Rd}\right)(y_1 y_8 + Nby_8 y_{10} + Nt(y_8)^2 + \Phi y_7)\right)$$

The boundary conditions become considering y_a be the left boundary, y_b be the right boundary

$$y_a(1),\ y_a(2)-\lambda,\ y_a(4),\ y_a(6),\ y_a(7)-1,\ y_a(9)-1$$

$$y_b(2)-1,\ y_b(5)-1,\ y_b(7),\ y_b(9)$$

Table 1: Comparison of solution $\Pr m = 0.5\ \ \beta = 0.1.\ Rd = 0.5\ \ Nb = 0.3\ \ Nt = 0.1\ \ Le = 5$

	$f''(0)$ **Present work**	$f''(0)$ **SRM** [23]	$f''(0)$ **RKG** [24]
0.1	0.462512600028002	0.462532849518307	0.462512534758035
0.2	0.443155034809943	0.443164986357953	0.443155102757022
0.4	0.375095416755509	0.375097915452026	0.375095448943384

5. Results and Discussion

The analytical solution considers the effects of the nanoparticle sheet velocity parameter, the magnetic field parameter, the Prandtl number, the magnetic Prandtl number, the thermal radiation parameter, the Lewis number, the Brownian motion parameter, the thermophoresis parameter, and the heat source/sink parameters on the heat and mass transfer properties of nanofluids have been examined.

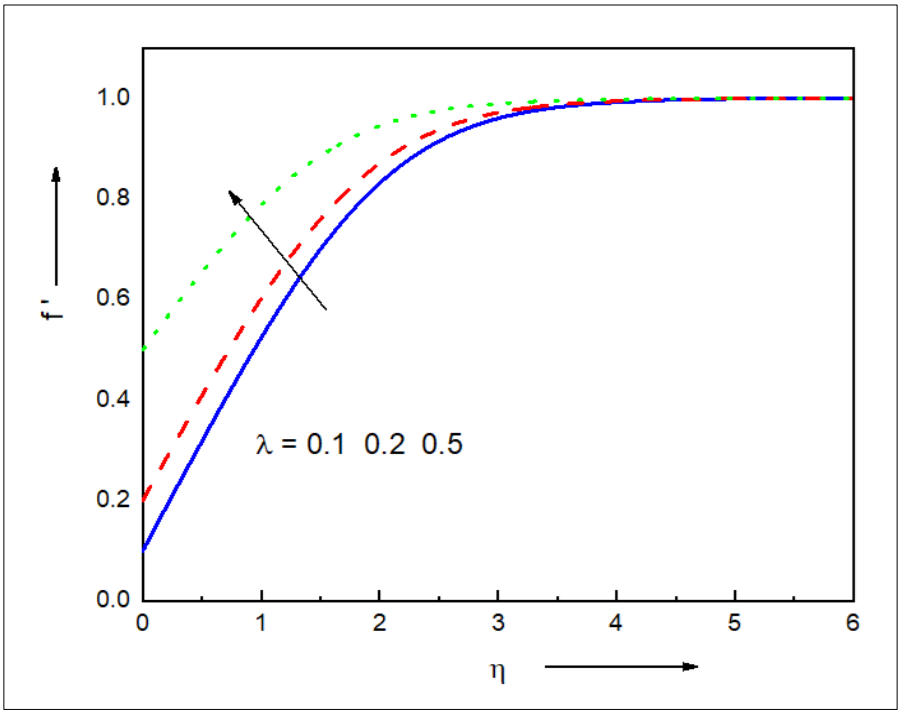

Fig 2: Velocity profiles for different values of sheet velocity parameter λ

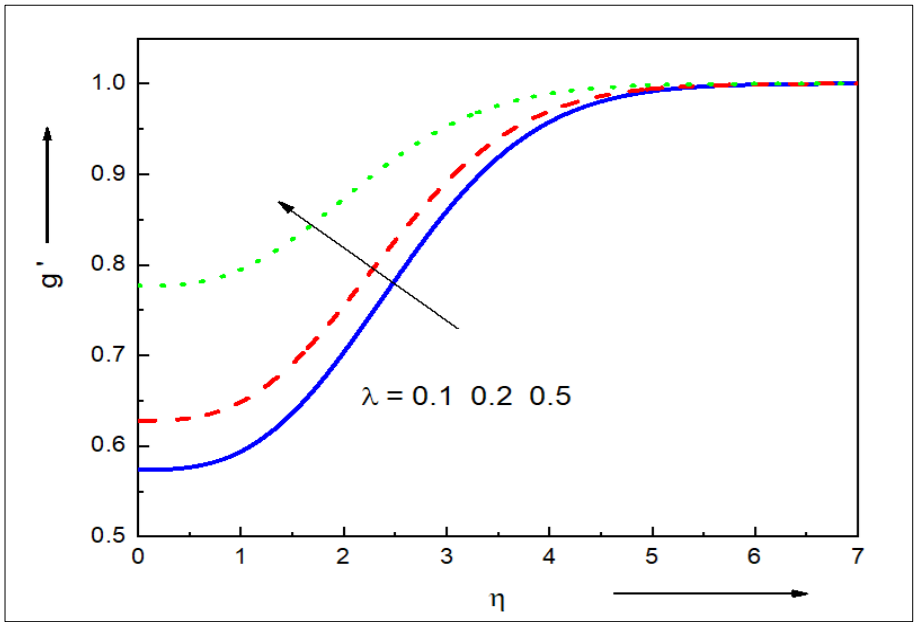

Fig 3: Induced magnetic stream function gradient for different values of sheet velocity parameter λ

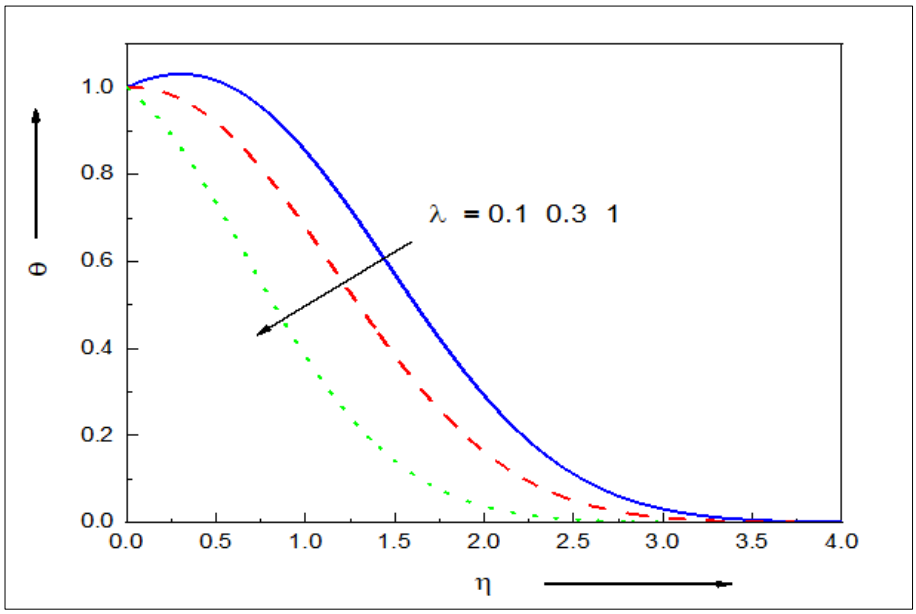

Fig 4: Temperature profile for different values of sheet velocity parameter λ

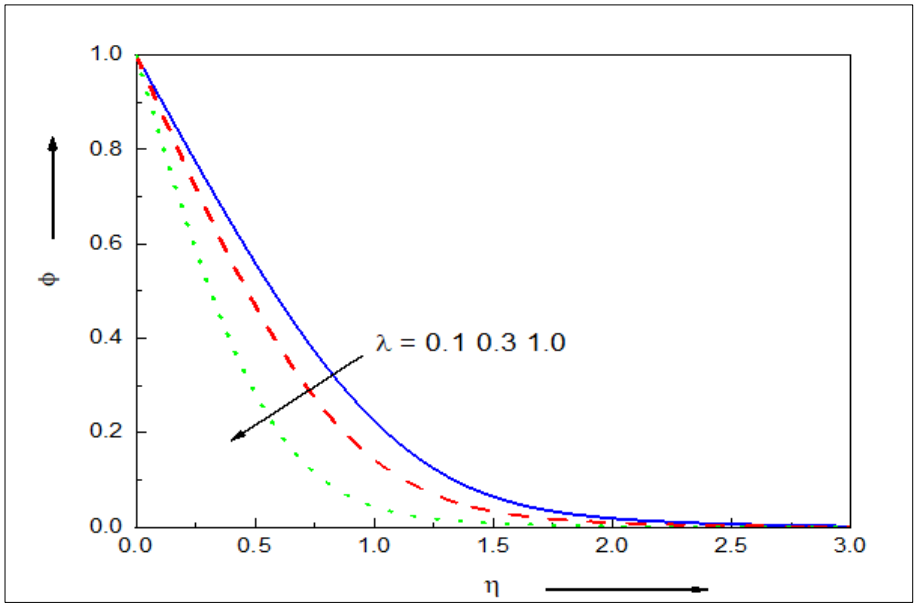

Fig 5: Nanoparticle concentration profiles for different values of sheet velocity parameter λ

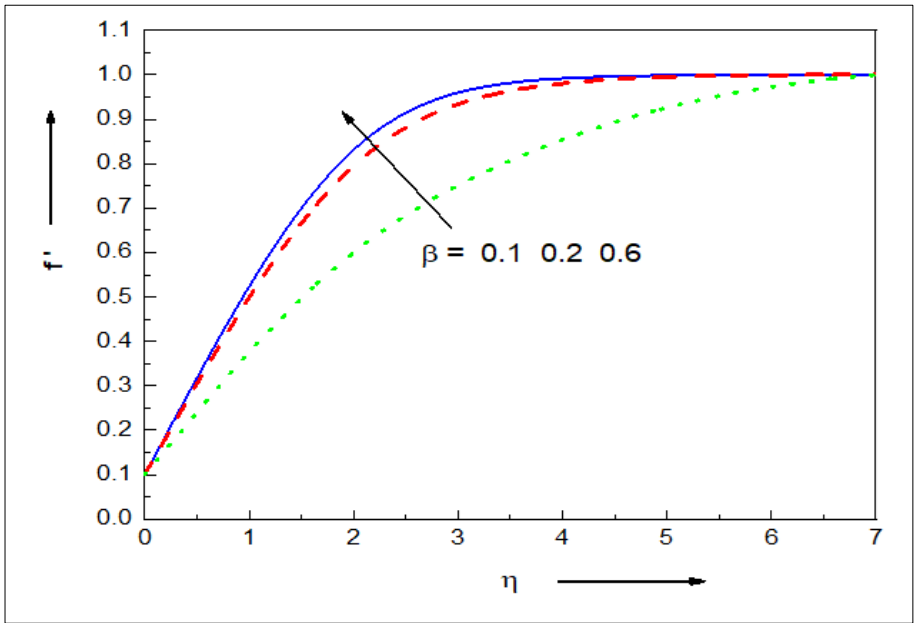

Fig 6: Velocity profiles for different values

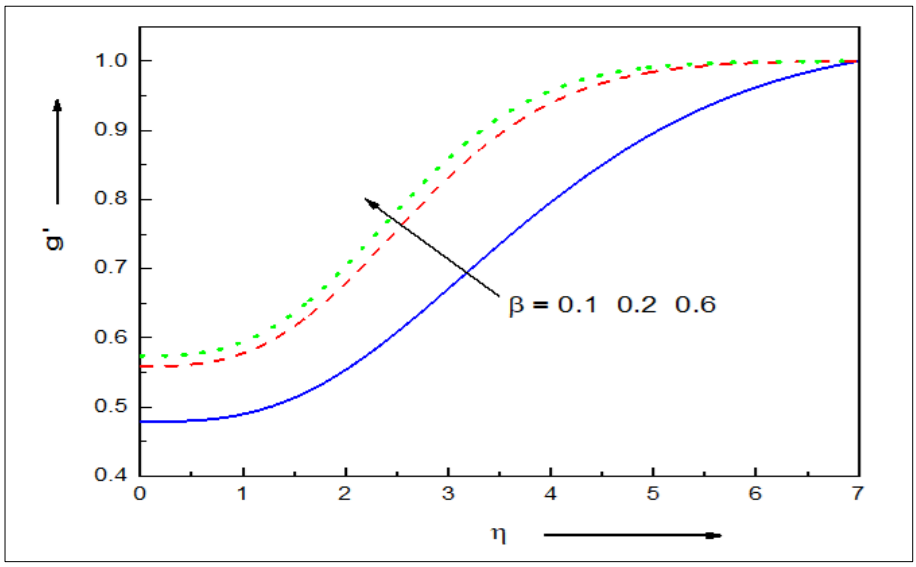

Fig 7: Induced magnetic stream function gradient for different values of magnetic force parameter β

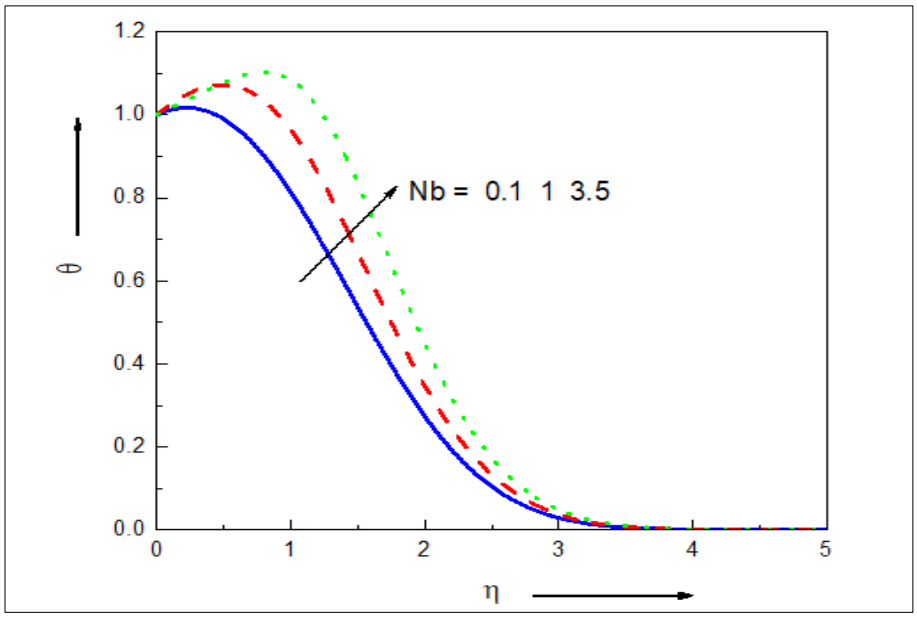

Fig 8: Temperature profile for different values of Brownian motion parameter Nb

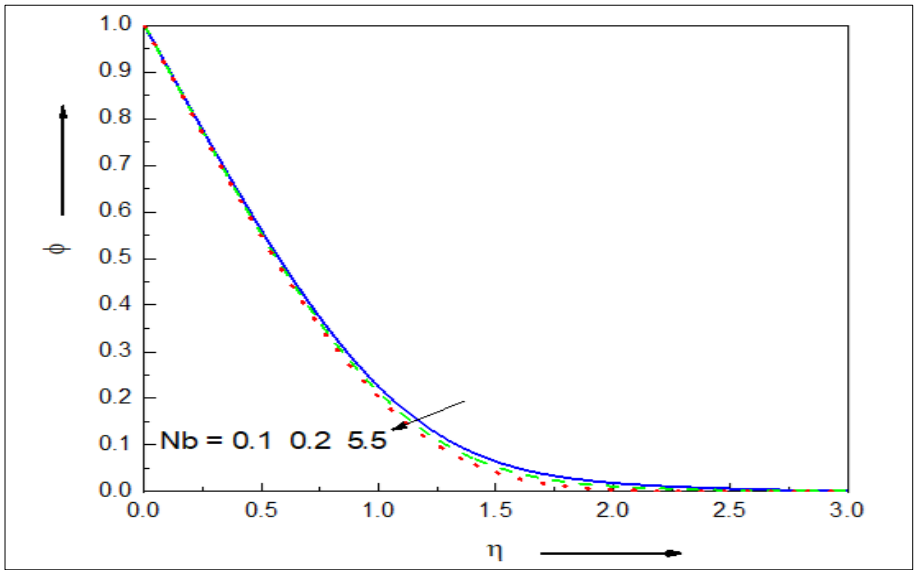

Fig 9: Nanoparticle concentration profiles for different values of Brownian motion parameter Nb

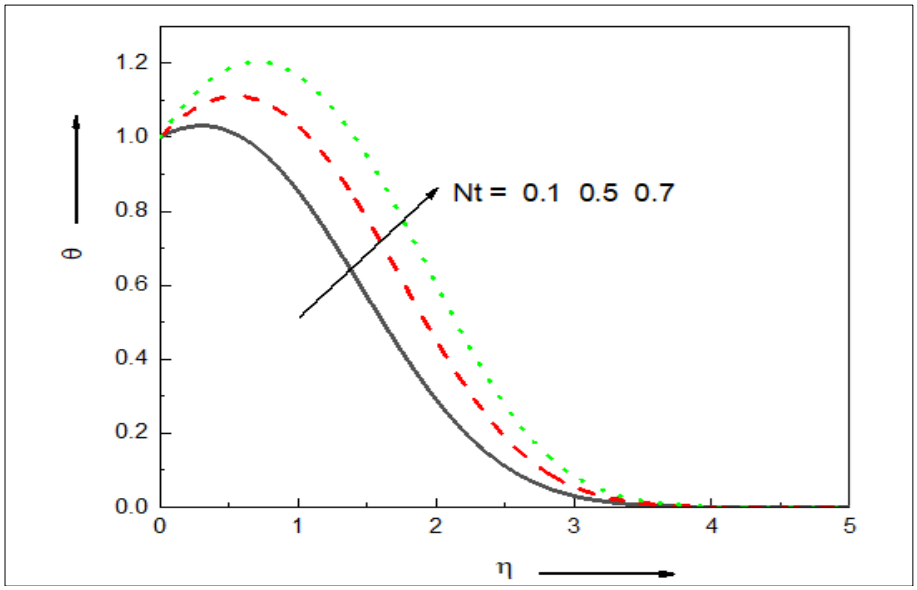

Fig 10: Temperature profile for different values thermophoresis parameter

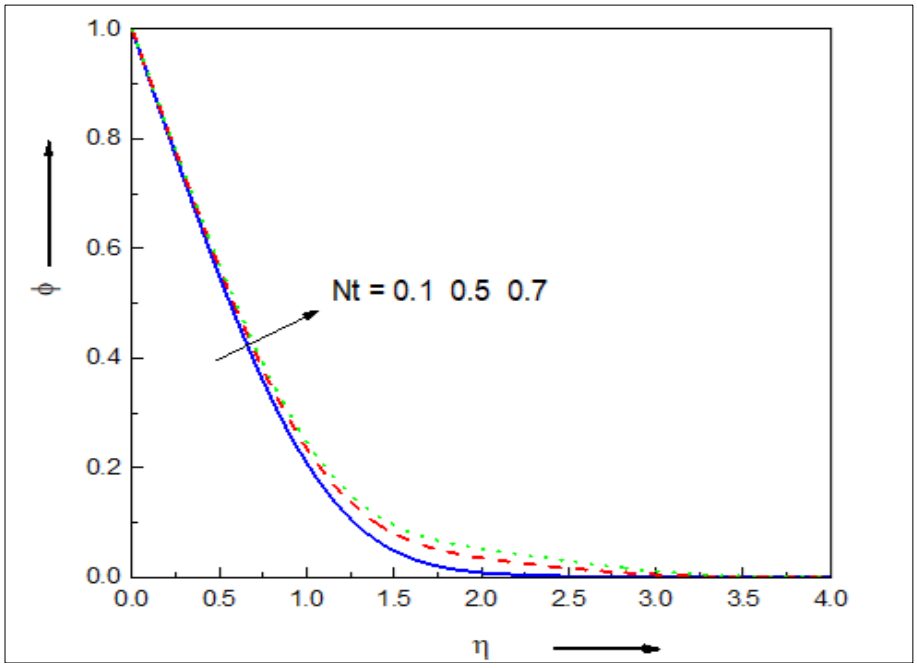

Fig 11: Nanoparticle concentration profiles for of different values of thermophorsis parameter Nt

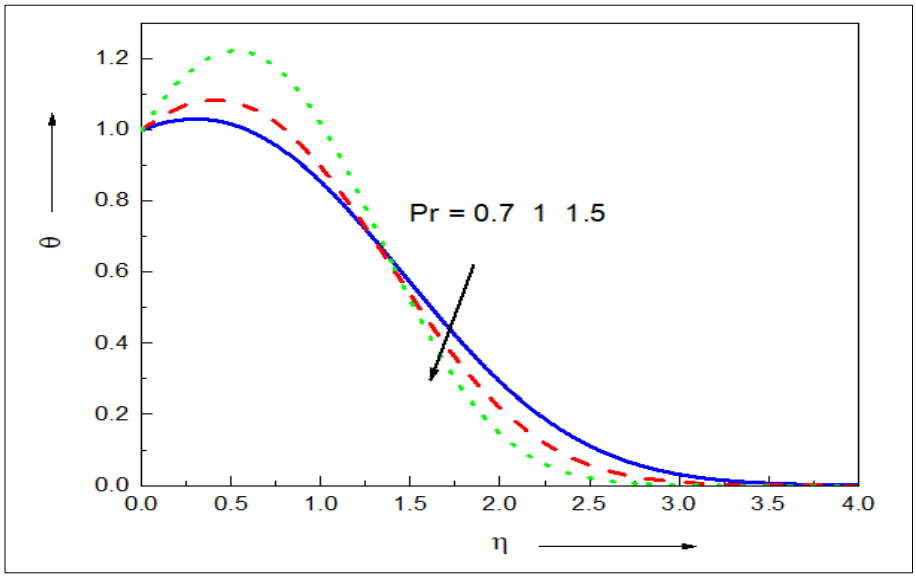

Fig 12: Temperature profile for different values of Prandtl number Pr

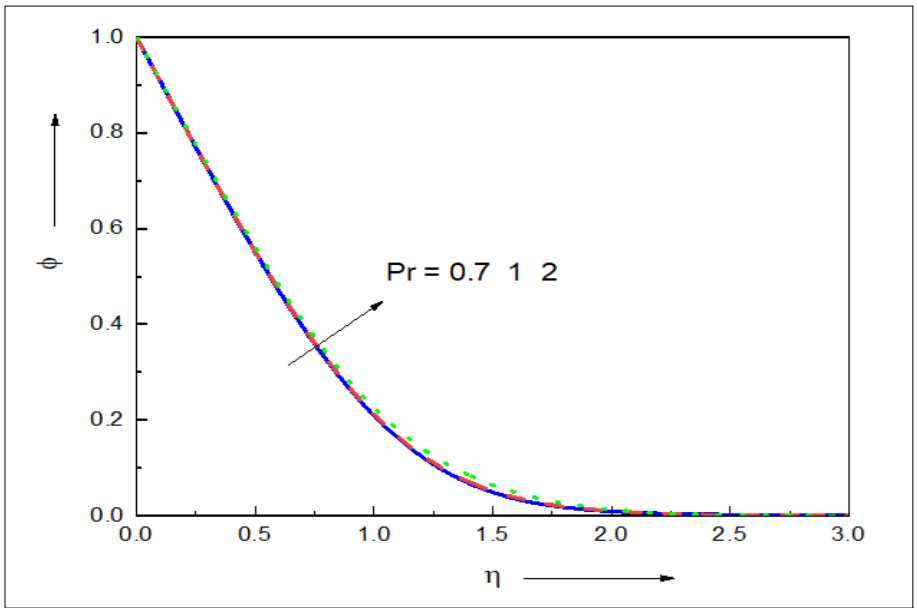

Fig 13: Nanoparticle concentration profiles for different values of Prandtl number Pr

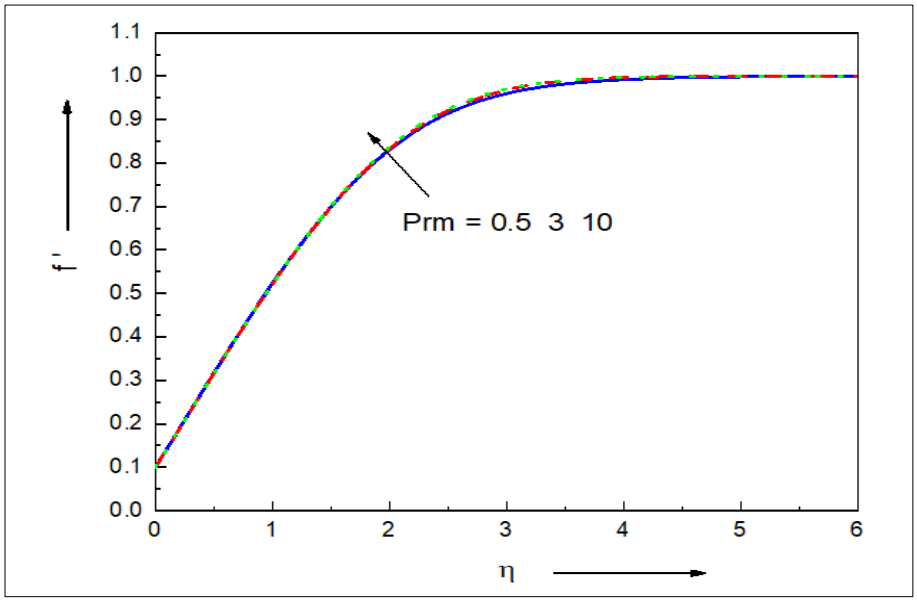

Fig 14: Velocity profiles for different values of magnetic Prandtl number P_{rm}

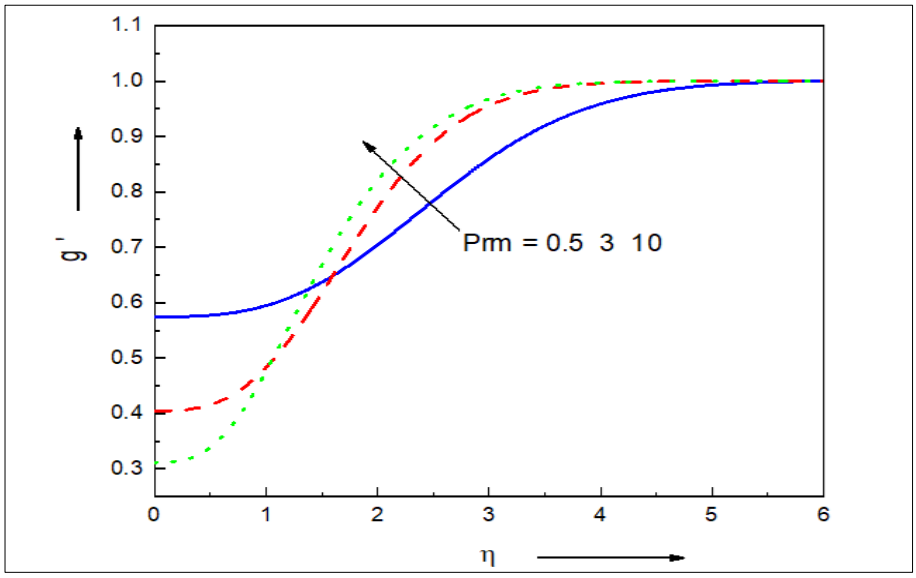

Fig 15: Induced magnetic stream function gradient for different values of magnetic prandtl number P_{rm}

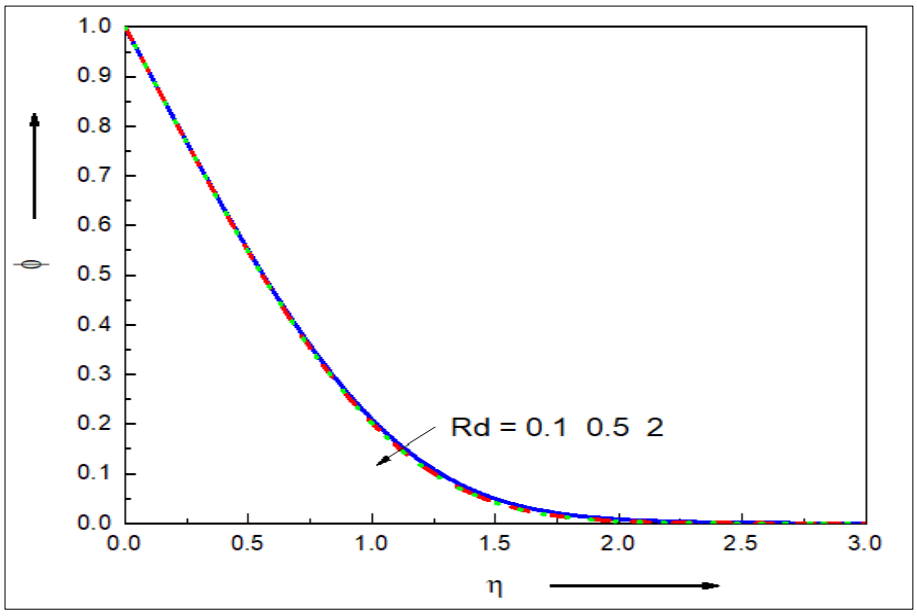

Fig 16: Nanoparticle concentration profiles for different values of Radiation parameter Rd

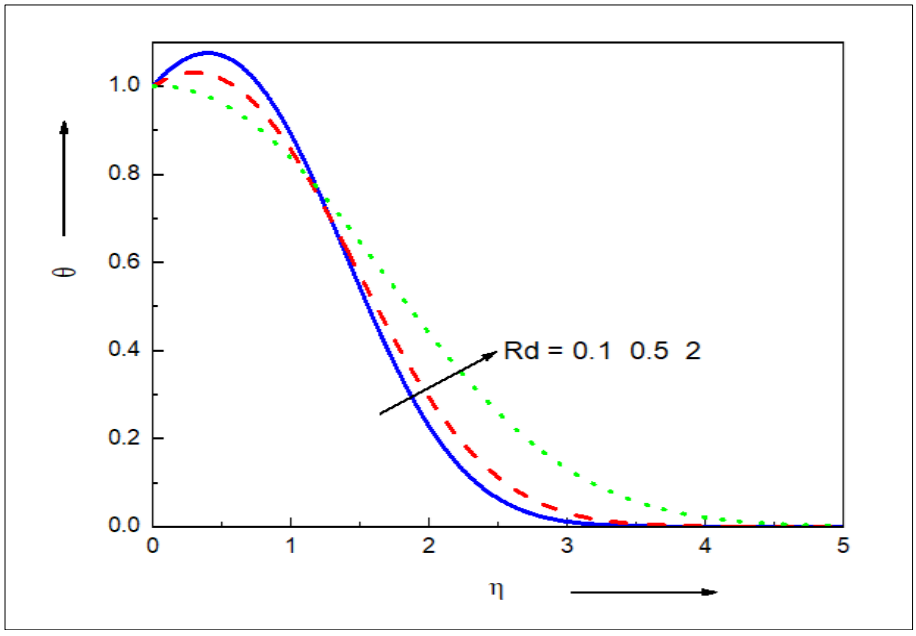

Fig 17: Temperature profile for different values of Radiation parameter Rd

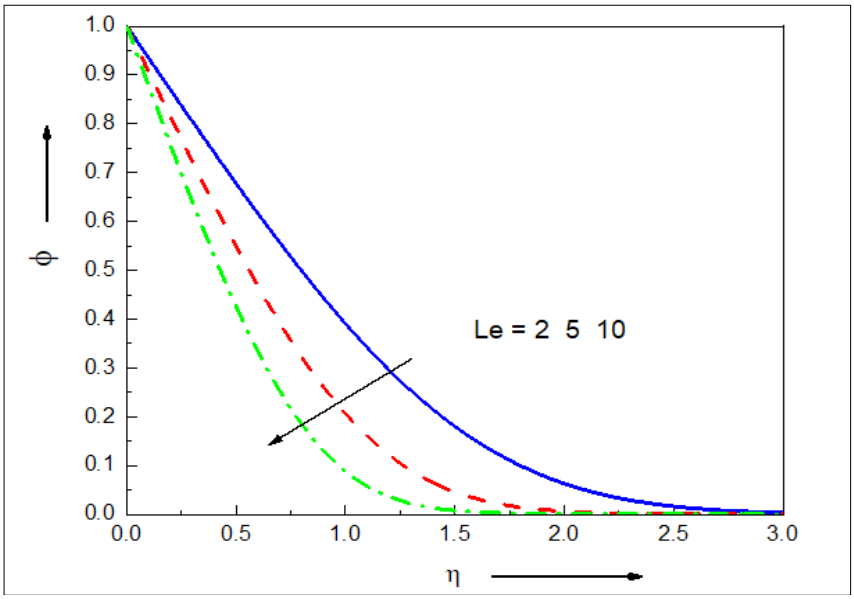

Fig 18: Nanoparticle concentration profiles for different values of Lewis number Le.

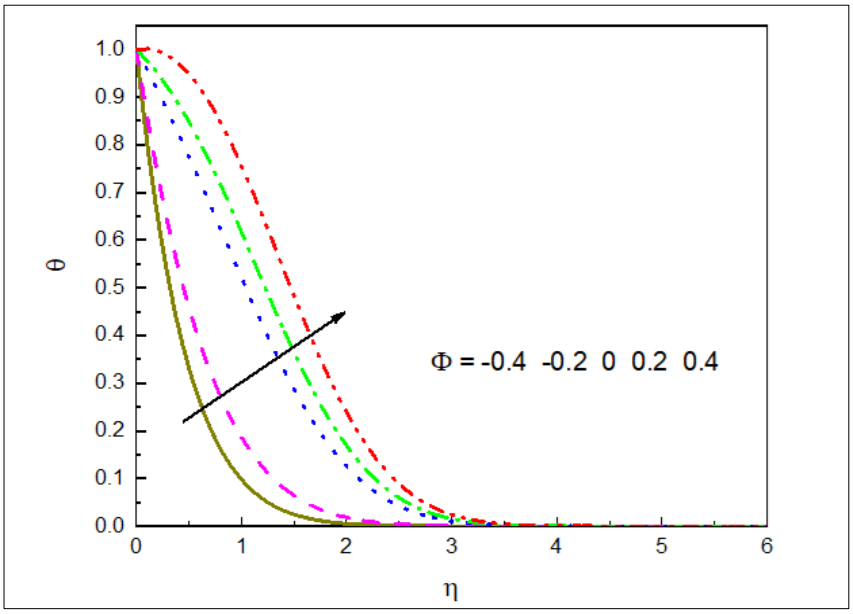

Fig 19: Temperature profile for different values of Source sink parameter

Table 2 shows the reduction of skin friction coefficient Cf, reduced Nusselt number Nu, and Sherwood number Sh It is observed that the heat transfer coefficient at the surface increases with increasing Prandtl number (thermal conductivity of magnetic nanofluid y The lower the temperature, the cooler the boundary layer and the better the heat transfer to the wall). In contrast, the mass transport rate decreases with increasing Prandtl number (increasing concentration of nanoparticles in the interfacial region and decreasing mass transport rate of nanoparticles to the wall). Increasing the Lewis number Le and the radiation parameter Rd increase the reduced Sherwood number at the limit. In contrast, the heat transfer coefficient at the boundary is reduced. It is also clear that increasing the moving surface parameter value λ decreases the skin friction on the wall panel, but does so for the Nusselt and Sherwood numbers.

Table 2: Skin Friction coefficient C_f, the reduced Nusselt number Nu and the reduced Sherwood number Sh with $\Pr m = 0.71$ $\beta = 0.1$

Pr	Le	Rd	λ	Nb	Nt	Φ	$f''(0)$	$-\theta'(0)$	$-\varphi'(0)$
1	2	1	0.1	0.1	0.1	0.5	0.437262014833274	0.000153834502078800	-0.573125869907670
2	2	1	0.1	0.1	0.1	0.5	0.437297961950999	0.189425205735967	-0.500437598038191
1	10	1	0.1	0.1	0.1	0.5	0.437261676094170	-0.00340054540136571	-1.18775125771533
1	2	2	0.1	0.1	0.1	0.5	0.437262380736984	-0.0310191563412717	-0.602877668432413
1	2	1	0.5	0.1	0.1	0.5	0.314654884179653	-0.201696561174432	-0.781719300270610
1	2	1	0.1	0.5	0.1	0.5	0.437262578109850	0.0554702343697229	-0.644625942856918
1	2	1	0.1	0.1	0.5	0.5	0.437261580467832	0.0660953939188788	-0.266044317373997
1	2	1	0.1	0.1	0.1	0	0.437244391594647	-0.418193170609861	-0.604511356478310

Table 3: Reduced Nusselt number Nu with $\Phi = 0.5$ $\Pr m = 0.5$ $\beta = 0.1.$ $Rd = 0.5$ $Nb = 0.3$ $Nt = 0.1$ $Le = 5$

λ	$-\theta'(0)$ **Pr = 0.71**	$-\theta'(0)$ **Pr = 1**	$-\theta'(0)$ **Pr = 1.5**
-0.3	-0.538976005701313	-1.13531208606193	-1.14721061945157
0.1	0.0107086451503400	-0.0509536675320768	-0.170592744497031
0.5	0.166220620370031	0.154195934275234	0.115172260635680
1	0.292394133412350	0.313386263614212	0.320375952035758
1.5	0.387950781071738	0.431542255715111	0.467787709947936
-0.3	0.467218577229261	0.528583861599185	0.586863839614828

Table 3 shows the heat transfer coefficient for various values of the Prandtl number Pr at other limited flow parameters. For negative wall velocities, the reduced Nusselt number decreases, but for positive wall velocities, it decreases steadily for all Prandtl numbers. Table 4 shows the reduced Sherwood number for various values of the Lewis number Le, all other parameters held constant. The decreasing Sherwood number decreases with increasing Lewis number and, for negative wall velocities, increases with a more pronounced Lewis number for positive wall velocities. Table 5 shows the effect of different magnetic force parameter β with different blade speed parameter λ on skin friction coefficient. It can be observed that the coefficient of skin friction decreased very rapidly with increasing values of these parameters.

Table 4: Reduced Sherwood number Sh with $\Phi = 0.5$ $\Pr m = 0.5$ $\beta = 0.1.$ $Rd = 0.5$ $Nb = 0.1$ $\Pr = 0.71$ $Nt = 0.3$

λ	$-\varphi'(0) Le = 1$	$-\varphi'(0) Le = 5$	$-\varphi'(0) Le = 10$
-0.3	0.213522934364599	0.182336221371764	0.100831489558115
0.1	0.468993970374211	0.920289016060568	1.21576294304712
0.5	0.606266245337930	1.34961959889375	1.88559736294214
1	0.738156545488644	1.75523297314625	2.50378862766948
1.5	0.847808252098130	2.08711179739332	3.00341840793416
2	0.943871768696439	2.37451149517341	3.43317578195023

Table 5: Skin Friction coefficient C_f , with $\Phi = 0.5$ $\Pr m = 0.5$ $Rd = 0.5$ $Nb = 0.3, Nt = 0.1$ $\Pr = 0.71$

λ	$f''(0)$ β **=0.1**	$f''(0)$ β **=0.2**	$f''(0)$ β **=0.3**
0.1	0.438076423254898	0.411970420513293	0.383506071157544
0.2	0.421662362982080	0.398649487057466	0.373551707821951
0.3	0.394849209290746	0.374768985955416	0.352849337147075
0.4	0.359081892034367	0.341860075797318	0.323038954254932
0.5	0.315387226579948	0.300996525217434	0.285248909171942
0.6	0.264535228985126	0.252974737721553	0.240307833641613
0.7	0.207127313635749	0.198412457193284	0.188851213478367
0.8	0.143646951591714	0.137803360102842	0.131384249907633
0.9	0.0744930143273016	0.0715528821003178	0.0683193893397657

Figure 2 shows the effect on the velocity profile for different values of the blade velocity parameter. It can be seen that an increase in the velocity parameter λ leads to an increase in the flow acceleration. Achieve a smooth profile with a free stream. Figure 3 shows the effect on the induced magnetic current for different values of the blade speed parameter. It can be seen that an increase in the velocity parameter increases the velocity of the flow-induced magnetic field. Asymptotically smooth profiles are obtained for free streams with sufficiently large infinite boundary conditions. Figure 4 shows the effect on the temperature profile for different values of the layer velocity parameter. This indicates that the nature of the curve due to the thermal boundary layer thickness decreases as the wall velocity parameter increases. Figure 5 shows the effect on the concentration profile for different values of the blade speed parameter. As the rate parameter increases, the curve decreases with the boundary layer thickness of the nanoparticle concentration.

Figure 6 shows the effect on the velocity profile for different values of the magnetic blade parameters. It is observed that the velocity field decreases, the thickness of the momentum boundary layer increases and the thickness of the magnetic boundary layer decreases. Figure 7 shows the effect on the induced magnet current for different values of the magnetic sheet parameters. It is observed that the induced magnetic current decreases, while the thickness of the pulse boundary layer increases and the thickness of the magnetic boundary layer decreases.

Figure 8 shows the effect on the temperature profile for different values of the Brownian motion parameter Nb. It can be seen that the temperature profile decreases as the Brownian motion parameter Nb increases. Achieve a smooth profile with a free jet. Figure 9 shows the effect on the concentration profile for different values of the Brownian motion parameter Nb. It can be seen that the Brownian motion parameter Nb decreases the velocity of the concentration profile. Figure 10 shows the effect on the temperature profile for different values of the thermophoretic parameter Nt. It can be seen that the temperature profile decreases as the thermophoretic parameter Nt increases. Achieve a smooth profile with a free jet. Figure 11 shows the effect on the concentration profile for different values of the thermophoretic parameter Nt. It can be seen that the thermophoretic parameter Nt leads to a slowing down of the concentration profile.

Figures 12 and 13 show the variation of temperature and nanoparticle concentration distribution as the Prandtl number Pr is varied. An increase in the Prandtl number Pr significantly reduces the temperature of the nanofluid and suppresses the thickness of the thermal boundary layer. The nanoparticle concentration profile shows a monotonic response to the Prandtl number. An increase in H. Pr promotes diffusion of nanoparticles and also increases the thickness of the boundary layer of nanoparticles concentration. Figure 14 shows the effect on the velocity profile for different values of the magnetic Prandtl number Prm. It can be seen that the flow acceleration increases as the magnetic Prandtl number Prm increases. Figure 15 shows the effect on the induced magnetic current for different values of the magnetic Prandtl number Prm. It can be seen that the velocity of the flow-induced magnetic field increases with an increase in the magnetic Prandtl number Prm.

Figure 16 shows the effect on the temperature profile for different values of the radiation parameter Rd, and it can be seen that an increase in the radiation parameter Rd leads to a decrease in the temperature profile. Figure 17 shows the effect on the nanoparticle concentration profile for different values of the radiation parameter Rd, showing that the radiation parameter Rd leads to a decrease in the concentration profile. Figure 18 shows the change in nanoparticle concentration profile with the Lewis number Le. At Le = 1, these velocities are equal and the boundary layer thicknesses of momentum and nanoparticle concentration are similar. Figure 19 shows the variation of the temperature profile with heat source/sink parameters. It can be seen that the temperature profile decreases as the heat source/sink parameters increase.

6. Conclusion

A mathematical study of Two-Dimensional MHD steady-state boundary laminar flow by thermal convection of a conducting nanoliquid across a smooth free-flow moving surface with heat source/sink is presented. The Buongiorno model was used, which takes into account Brownian diffusion and thermophoretic results. The flow and heat transfer partial differential equations were transformed into coupled nonlinear ordinary differential equations using appropriate similarity transformations. The coupled nonlinear momentum and thermal boundary layer equations are computed numerically using MATLAB bvp4c. The solutions obtained are linked to the literature and conclusions are drawn. Changes in skin friction coefficient, heat transfer coefficient, mass transfer coefficient, velocity, and induced magnetic field, temperature, and nanoparticle volume fraction profiles are displayed in tabular and graphical form for various values of physical parameters. From this study, some key findings are summarized as follows.

1. It is observed that the Velocity and induced magnetic field profiles decrease with an increase in magnetic body force parameters.
2. Increasing in the magnetic parameter, thermophoresis parameter, and radiative parameter thickness is enhanced in boundary layer. In contrast, they are diminished with more incredible wall velocity, Brownian motion, and Prandtl numbers.
3. Induced magnetic field stream function is affected by reciprocating the magnetic Prandtl number Prm compared with the skin-friction and heat transfer coefficients.
4. The nanoparticle concentration improves with greater values of thermophoresis and Prandtl number, but it is suppressed with increasing moving wall, Brownian motion, radiative, and Lewis numbers.
5. The heat source/sink parameter suppresses the temperature profile and decrease with higher values.

The work can be continued by selecting several more models of different non-Newtonian liquids and nanoliquids made with different combinations of nanoparticles. However, attention is limited to Newtonian nanofluids. This study, which will be published soon, explores the rheological behavior of nanofluids, including viscoelastic [28] and viscoplastic [29] models. The results obtained in such studies are of great benefit in dealing with nanofluidic coating streams, energy conservation, magneto therapy and biomedical fields.

References

1. Choi SUS, Eastman JA. Enhancing thermal conductivity of fluids with nanoparticles. Argonne National Laboratory; 1995. Report No.: ANL/MSD/CP-84938.
2. Udin M, Anwar B, Ahmed I. Radiative convective nanofluid flow past a stretching/shrinking sheet with slip effects. Journal of Thermophysics and Heat Transfer. 2016. DOI:10.2514/1.T4372.
3. Mahanthesh B, Gireesha BJ, Athira PR. Radiated flow of chemically reacting nanoliquid with an induced magnetic field across a permeable vertical plate. Results in Physics. 2017;7:2599-2607. DOI:10.1016/j.rinp.2017.07.010.
4. Ali A, Khan HS, Saleem S, Hassan M. EMHD nanofluid flow with radiation and variable heat flux along a slender stretching sheet. Nanomaterials. 2022;12:3872. DOI:10.3390/nano12213872.
5. Poply V. Heat transfer in a MHD nanofluid over a stretching sheet. In: Heat Transfer - Design, Experimentation and Applications. InTechOpen; 2011.
6. Jafar AB, Shafie S, Ullah I. MHD radiative nanofluid flow induced by a nonlinear stretching sheet in a porous medium. Heliyon. 2020;6:e04201. DOI:10.1016/j.heliyon.2020.e04201.
7. Srisailam B, Reddy SR, Narender G, Malga BS. Flow and heat transfer analysis of MHD nanofluid due to convective stretching sheet. Indian Journal of Science and Technology. 2022;15(44):2393-2402. DOI:10.17485/IJST/v15i44.1006.
8. Sharma S. MHD boundary layer flow past an exponentially stretching sheet with Darcy-Forchheimer flow of nanofluids. Indian Journal of Science and Technology. 2022;15(33):1594-1604. DOI:10.17485/IJST/v15i33.607.
9. Goud BS, Srilatha P, Shekar RMN. Soret effects on free convection nanofluid flows due to a stretching sheet. Journal of Nanofluids. 2023;12:202-210.
10. Daniel YS, Aziz ZA, Ismail Z, Salah F. Thermal stratification effects on MHD radiative flow of nanofluid over nonlinear stretching sheet with variable thickness. Journal of Computational Design and Engineering. 2018;5(2):232-242.
11. Saeed A, Kumam P, Nasir S, Gul T, Kumam W. Nonlinear convective flow of thin film nanofluid over an inclined stretching surface. Scientific Reports. 2021;11:18410. DOI:10.1038/s41598-021-97576-x.

12. Waini I, Ishak A, Pop I. Mixed convection flow over an exponentially stretching/shrinking vertical surface in a hybrid nanofluid. Alexandria Engineering Journal. 2020;59(3):1881-1891.
13. Nabil TB, Raafat RR, Mohammed YA, Vivian A. Effect of induced magnetic field on non-Newtonian nanofluid motion through boundary layer with gyrotactic microorganisms. Thermal Science. 2022;26(1B):411-421. DOI:10.2298/TSCI200408189E.
14. Odhiambo OW, Kimathi M, Wainaina M. Effects of induced magnetic field on electrically conducting Oldroyd-B nanofluid flow over a perforated linearly extending surface. Global Journal of Pure and Applied Mathematics. 2019;15(5):623-636.
15. Waini I, Ishak A, Pop I. Hybrid nanofluid flow induced by an exponential shrinking sheet. Chinese Journal of Physics. 2019. DOI:10.1016/j.cjph.2019.12.015.
16. Anwar MI, Firdous H, Zubaidi A, Nadeem A, Nadeem S. Computational analysis of induced magnetohydrodynamic non-Newtonian nanofluid flow over nonlinear stretching sheet. Journal of Engineering Tribology. 2022;47:1-17. DOI:10.1177/1468678321107271.
17. Alblawi A, Malik MY, Nadeem S, Abbas N. Buongiorno's nanofluid model over a curved exponentially stretching surface. Processes. 2019;7:665. DOI:10.3390/pr7100665.
18. Roşca NC, Roşca AV, Hassan EA, Pop I. Flow and heat transfer past a stretching/shrinking sheet using modified Buongiorno nanoliquid model. Mathematics. 2021;9:3047. DOI:10.3390/math9233047.
19. Aldabesh A, Hossain M, Khatun N, Riahi A, Khan SU, Talu I. Thermal variable conductivity features in Buongiorno nanofluid model between parallel stretching disks. Case Studies in Thermal Engineering. 2021;23:100820. DOI:10.1016/j.csite.2020.100820.
20. Kerur SB, Tawade JV, Biradar M, Manvi BK. Effect of non-uniform heat source/sink for Casson nanofluid over porous stretching sheet. Journal of Engineering Sciences. 2020;11.
21. Thiagarajan M, Kumar MD. Heat source/sink and chemical reaction effects on MHD radiative nanofluid over porous exponentially stretching sheet. International Journal of Basic Sciences and Applied Computing. 2019;2(7).
22. Misra S, Kamatam G. Effect of magnetic field, heat generation and absorption on nanofluid flow over a nonlinear stretching sheet. Beilstein Journal of Nanotechnology. 2020;11:976-990. DOI:10.3762/bjnano.11.82.
23. Umavathi JC, Patil SL, Mahanthesh B, Beg OA. Unsteady squeezing flow of magnetized nanolubricant between parallel disks with Robin boundary condition. Proceedings of the Institution of Mechanical Engineers, Part N. 2020. DOI:10.1177/23977914211036562.
24. Nima NI, Alshuraiaan B, Ferdows M. Mixed convection flow along vertical thin needles containing gyrotactic microorganisms. 2021. DOI:10.21203/rs.3.rs-753328/v1.
25. Akter S, Ferdows M, Beg TA, Beg OA, Kadir A, Sun S. Spectral relaxation computation of electroconductive nanofluid convection flow from a moving surface. Journal of Computational Design and Engineering. 2021;8(4):1158-1171. DOI:10.1093/jcde/qwab038.
26. Shateyi S, Prakash J. A new numerical approach for MHD laminar boundary layer flow of nanofluids over a moving surface. Boundary Value Problems. 2014;2014:2.
27. Chamkha AJ. Hydromagnetic natural convection from an isothermal inclined surface. International Journal of Engineering Science. 1997;35:975-986.
28. Rana P, Bhargava R, Beg OA, Kadir A. Finite element analysis of viscoelastic nanofluid flow. International Journal of Applied and Computational Mathematics. 2017;3(2):1421-1447.
29. Thumma T, Mishra SR, Beg OA. ADM solution for Cu/CuO-water viscoplastic nanofluid transient slip flow. Journal of Applied and Computational Mechanics. 2020;6:1-15.